Journal of Crystal Growth 378 (2013) 319–322

Contents lists available at SciVerse ScienceDirect

Journal of Crystal Growth

journal homepage: www.elsevier.com/locate/jcrysgro

Control of threading dislocation density at the initial growth stage of AlN on c-sapphire in plasma-assisted MBE

D.V. Nechaev*, P.A. Aseev, V.N. Jmerik, P.N. Brunkov, Y.V. Kuznetsova, A.A. Sitnikova, V.V. Ratnikov, S.V. Ivanov

Ioffe Physical-Technical Institute, Polytekhnicheskaya 26, St. Petersburg 194021, Russia

ARTICLE INFO

Available online 5 January 2013

Keywords:
A1. Dislocation
A3. Molecular beam epitaxy
A3. Migration enhanced epitaxy
B2. Semiconducting aluminium compounds

ABSTRACT

Crystalline properties of (1–2)-μm-thick AlN buffer layers grown by plasma-assisted molecular-beam epitaxy (PA MBE) on c-Al_2O_3 substrates with different AlN nucleation layers have been studied. The best quality layers are obtained on 50-nm-thick nucleation AlN layers grown by a migration enhanced epitaxy (MEE) at substrate temperature of 780 °C. In this case the buffer layers possess the lowest FWHM values of the symmetric AlN(0002) and skew symmetric AlN(10–15) x-ray rocking curve peaks of 469 and 1025 arcsec, respectively, which correspond to the screw and edge threading dislocation densities of 4.7×10^8 cm^{-2} and 5.9×10^9 cm^{-2}. This improvement seems to be related with the larger diameter of the flat-top grains in the AlN nucleation layers grown in the MEE mode at high substrate temperatures.

1. Introduction

AlGaN-based sources of deep ultraviolet (UV) spontaneous and stimulated emission as well as UV-photodetectors are of great interest due to their numerous potential applications in systems of water and air UV disinfection, covert communication, in photosensitive technologies etc. [1–3]. However, deterioration of structural quality of the AlGaN epilayers with increasing the Al content, when growing on sapphire substrates, as well as absence of the commercially available homoepitaxial substrates are the serious problems preventing fast elaboration of semiconductor deep UV optoelectronics. The AlGaN-based heterostructures grown on the conventional c-Al_2O_3 substrates usually exhibit high densities of the screw and edge threading dislocations (TDs) up to $\sim10^{10}$ cm^{-2}. The mechanisms of generation and reduction of TDs in the AlN buffer layers (BL) nucleated on c-Al_2O_3 substrates were studied in detail in the AlGaN-based structures grown by high-temperature (> 1000 °C) MOVPE technology, which has provided a significant progress in the manufacturing deep UV-optoelectronic devices by this technology [4–6].

Plasma-assisted molecular-beam epitaxy (PA MBE) was also employed to fabricate successfully the AlGaN-based spontaneous and laser UV emitters of reasonable quality [7–9]. It has demonstrated the high potential in realization of quantum-confined heterostructures due to the precise control of epitaxial growth on the atomic level. However, further progress in PA MBE of these materials can be achieved only via thorough study of the TDs suppression in the AlGaN/AlN/c-Al_2O_3 heterostructures grown at the relatively low substrate temperature ($T_S < 800$ °C) and low-pressure PA MBE environment. In our previous study, a two-step AlN buffer layer consisting of the 30-nm-thick low temperature and 250-nm-thick high-temperature layers enabled reducing the TD density down to 10^9–10^{10} cm^{-2} [8]. Recently, similar results with minimum TD densities in the range of 5.5×10^9–10^{10} cm^{-2} have been demonstrated in $Al_xGa_{1-x}N$ layers (x below 0.4) grown at the relatively high temperature (T_S=870 °C) by ammonia-MBE [10]. In addition, the growth temperature dependences of the TD densities in the 250-nm-thick AlN films grown on Si(1 1 1) substrates by PA MBE have been reported [11].

In this paper, we study the generation and filtering of the screw and edge TDs in (1–2)-μm-thick AlN BLs grown on the AlN/c-Al_2O_3 nucleation layers (NLs) fabricated by the both conventional and MEE PA MBE at different substrate temperatures.

2. Experiment

The samples were grown by PA MBE on c-Al_2O_3 substrates annealed and nitridated at the temperatures of T_S=800 °C and 700 °C, respectively. Fig. 1a illustrates variation of growth conditions across the thickness for the studied types of AlN NLs. The conventional MBE mode was used for growing the 30 nm-thick AlN NLs in the first two samples. They were grown at the same N-rich conditions with the flux ratio of $F_{Al}/F_N\sim0.7$ but different substrate

* Corresponding author. Tel.: +7 812 2927124; fax: +7 812 297 36 20.
E-mail address: nechayev@mail.ioffe.ru (D.V. Nechaev).

0022-0248/$ - see front matter © 2013 Elsevier B.V. All rights reserved.
http://dx.doi.org/10.1016/j.jcrysgro.2012.12.080

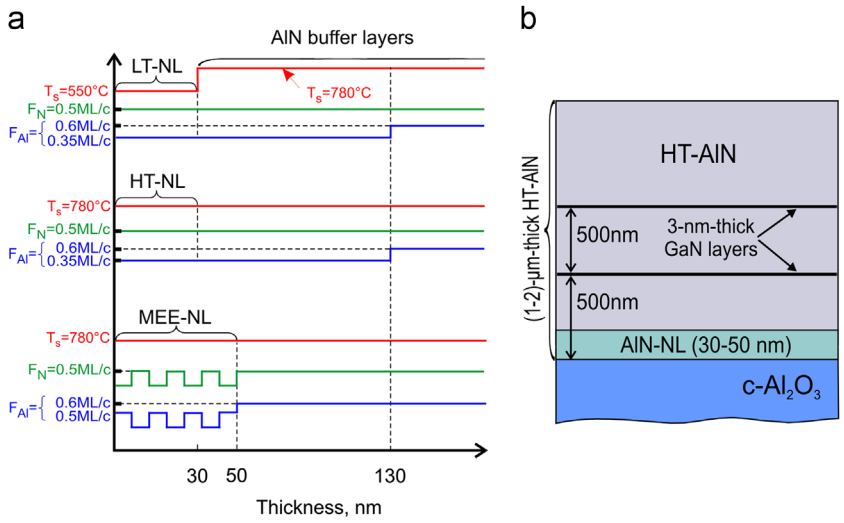

Fig. 1. (a) Growth conditions of the AlN BLs containing different AlN NLs (b) The sketch of the AlN BL samples.

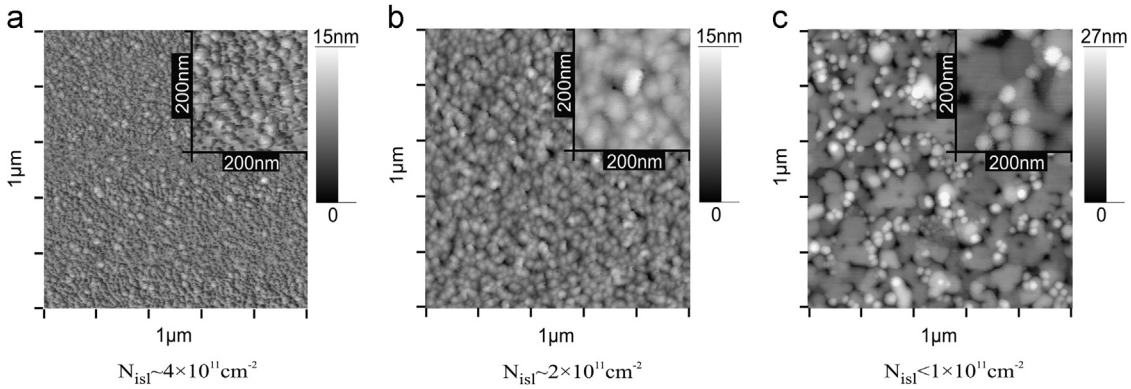

Fig. 2. AFM images of the thin AlN reference layers grown atop of different NLs: (a) 30-nm-thick LT NL, (b) 30-nm-thick HT NL and (c) 50-nm-thick MEE NL.

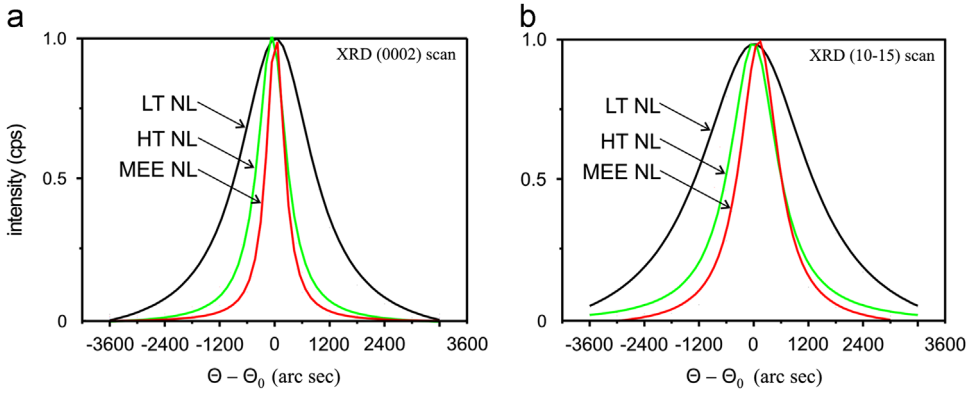

Fig. 3. XRD rocking curves of (a) AlN(0002) and (b) AlN(10–$\bar{1}$5) scans for the AlN buffer layers grown on different NLs.

temperatures (T_S) – low temperature T_S=550 °C (LT-NL) and high temperature T_S=780 °C (HT-NL). The high T_S=780 °C was also used during growth of the 50-nm-thick AlN NL in the third sample, while its growth mode was changed to a migration enhanced epitaxy (MEE) with alternating supplying of the Al and N fluxes for 30 s each (MEE-NL). On top of all the NLs, the (1–2)-μm-thick AlN BLs were grown at high T_S=780 °C but different stoichiometric conditions. Overall structure of AlN BLs is shown in Fig. 1b. For LT-NL and HT-NL samples, the N-rich conditions stimulating a 3D growth mechanism were used for the BL growth until its thickness reached ~130 nm. Then Al-rich conditions ($F_{Al}/F_N > 1.2$) with short periodic Al flux interruptions and continuous nitrogen flux were employed to provide the droplet-free and atomically smooth AlN films with a thickness up to 2 μm and rms < 2 ML over 4 μm^2 [12]. For the MEE-NL sample, the Al-rich growth of the AlN BL started immediately after the NL growth. Two 3-nm-thick strained GaN layers were inserted consequently in the BLs of all the structures to provide additional filtering of TDs. In addition, the (30–390)-nm-thick AlN reference layers with the same NLs as in the thick AlN BLs were grown on c-Al_2O_3 to evaluate the surface morphology and the stress relaxation in the layers by

atomic force microscopy (AFM) and x-ray diffraction (XRD) analysis, respectively.

Reflection high energy electron diffraction (RHEED) and laser reflectometry (LR) were used for in situ monitoring of the surface morphology and growth rate of the layers. XRD analysis of both symmetric AlN(0002) and skew symmetric AlN(10–$\bar{1}$5) reflexes was applied to estimate densities of the screw and edge TDs in the AlN BLs in accordance with the approach proposed by Moram and Vickers in Ref. [13]. The crystalline properties of the AlN layers were evaluated using transmission electron microscope (TEM).

3. Results and discussion

Fig. 2 shows AFM surface images of the thin AlN reference layers with different NLs. The surface of LT-NL sample shows the highest islands density of $\sim 4\times10^{11}\,cm^{-2}$ and the smallest lateral size, while HT-NL and MEE-NL samples exhibit larger islands with densities of $\sim 2\times10^{11}\,cm^{-2}$ and below $10^{11}\,cm^{-2}$, respectively. The enlargement of the grain sizes is explained by an increase of adatom mobilities on sapphire surface with the T_S rising. Moreover, this effect was much more pronounced in the MEE-NL sample due to the much larger time available for nucleation of the AlN nanoislands.

The rocking curves of the XRD reflexes for all AlN BLs grown on the different NLs are presented in Fig. 3. The widest AlN(0002) reflex with FWHM of 1944 arcsec (Fig. 3a) corresponding to the density of screw TDs $N_{screw}=8.2\times10^{9}\,cm^{-2}$ was measured for the structure with the LT-NL. The BLs with HT- and MEE-NLs exhibit much narrower AlN(0002) peaks with FWHM of 774 arcsec ($N_{screw}=1.2\times10^{9}\,cm^{-2}$) and 469 arcsec ($N_{screw}=4.7\times10^{8}\,cm^{-2}$), respectively. For another AlN(10–$\bar{1}$5) reflex, a similar dependence is revealed: the widest FWHM of 2910 arcsec ($N_{edge}=4.7\times10^{10}\,cm^{-2}$) is in the layer with LT-NL, while narrower FWHM values of 1194 arcsec ($N_{edge}=8.9\times10^{9}\,cm^{-2}$) and 1025 arcsec ($N_{edge}=5.9\times10^{9}\,cm^{-2}$) are measured in the layers with HT- and MEE-NLs, as shown in Fig. 3b. It should be noted that no cracking and buckling phenomena were observed in the AlN BLs undergoing the compressive strain.

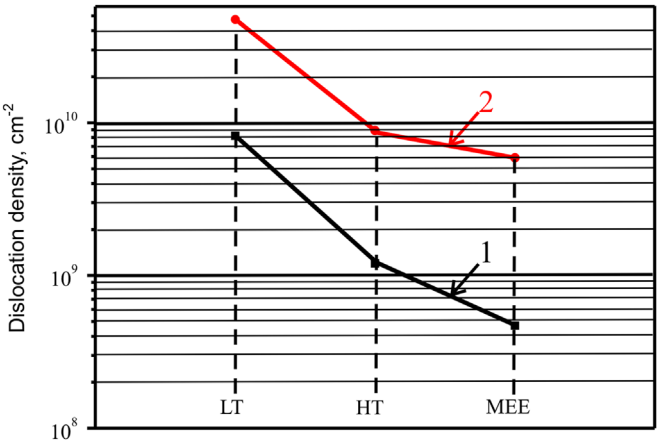

Fig. 4. The screw (1) and edge (2) threading dislocation densities versus the AlN NLs employed.

The densities of the screw and edge TDs, determined from the XRD analysis, are summarized in Fig. 4 as dependent on the type of the AlN NLs. These results were confirmed by TEM study, which revealed the lowest density of the screw TDs ($<8\times10^{8}\,cm^{-2}$) for the layers with MEE-NL. Additionally, substrate curvature radius (R) measured by XRD in the 390-nm-thick AlN reference layers revealed the complete stress relaxation ($R=+317$ m) in the sample with the LT-NL, while the layer with MEE-NL demonstrated an incomplete relaxation ($R=+26$ m).

The obtained data clearly show that the grain size of the AlN NLs plays a significant role in lowering the densities of both screw and edge TDs in AlN BLs. The best structural quality of the AlN layer which is comparable with the state-of-the-art quality of the AlN films grown by high-temperature MOVPE technology [14], was revealed in the sample with MEE-NL. This can be explained by the fact that TDs are generated mainly at the grain boundaries during island coalescence processes and the larger initial size of the nuclei results in reduction of the density of both the boundaries and TDs.

For additional reduction of the TDs during the growth of AlN BL we used other approaches including (i) the transition from 3D to 2D growth mode and (ii) insertion of the strained ultra-thin (~3 nm) GaN layers. Fig. 5 shows the cross-section bright-field TEM images (taken at $\boldsymbol{g}=\{0002\}$ and $\boldsymbol{g}=\{01\bar{1}0\}$ two-beam imaging conditions) of the AlN BL (with LT NL) grown at the varied stoichiometric conditions. One can see the significant density reduction of the both screw and edge TDs, propagating from the AlN/Al_2O_3 interface, in the region corresponding to the transition from 3D to 2D surface morphology (at ~130 nm from the interface). This can be explained by enhancing growth in lateral directions, induced by the Al surface adlayer, which facilitates bending of the TDs. The thin GaN layers inserted in the AlN BL reveal the analogous effect of TDs inclination (up to 90°) followed by their fusion and annihilation. Moreover, the compressive strain during the growth of AlN BL enforces the interaction of the TDs, leading to their reduction, since inclination angle of dislocation line is proportional to the strain in the layer as it has been shown in Ref. [15].

Summarizing, since the ultrathin strained GaN layers were inserted in all the AlN BLs, and the best structural quality was

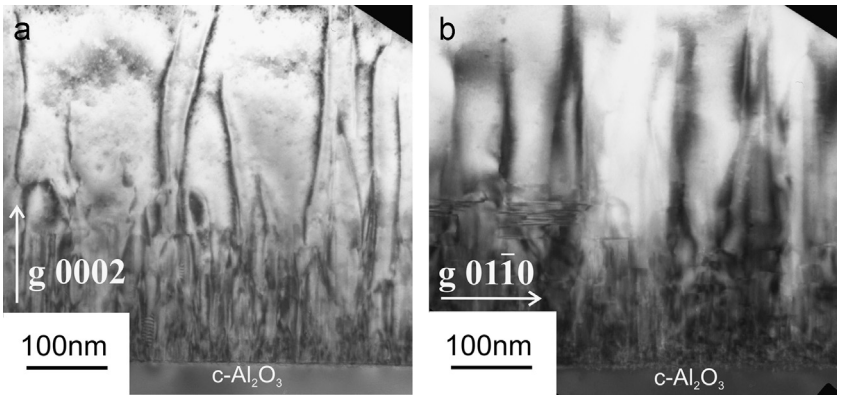

Fig. 5. Cross-section bright-field TEM image with (a) $\boldsymbol{g}=0002$ and (b) $\boldsymbol{g}=01\text{–}10$ of the AlN BLs grown on the LT NL.

revealed in the BL with MEE-NL, one can conclude, that the lateral grain size in the NL plays the most important role in reduction of TDs in comparison with the effect of the 3D to 2D growth mode transition employed in two other BLs.

4. Conclusion

In this paper, the structural quality of the thick AlN buffer layers grown on c-sapphire has been studied as dependent on the growth temperature (550° and 780 °C) and growth mode (conventional MBE or MEE mode) of the (30–50)-nm-thick AlN nucleation layers. The AlN buffer layer with the lowest screw and edge TD densities ($4.7\times10^8\,cm^{-2}$ and $5.9\times10^9\,cm^{-2}$, respectively) has been achieved in the structure with 50-nm-thick high temperature MEE nucleation layer followed by the high temperature thick AlN buffer layer grown under the Al-rich conditions with periodic Al flux interruptions. The significant reduction of the TD densities in the sample with the MEE NL is a result of action of several factors, with the enhanced initial lateral grain size in the NL being the most important.

Acknowledgements

The work is supported in part by RFBR, Program of RAS "Novel materials and structures" and Project KAST-SIPH/2. The authors acknowledge the assistance of the Joint Research Center "Material science and characterization in advanced technology" under financial support of the Ministry of Education and Science of the RF.

References

[1] H. Yoshida, M. Kuwabara, Y. Yamashita, K. Uchiyama, H. Kan, Phys. Stat. Sol. A 208 (2011) 1586.
[2] S. Hwang, D. Morgan, A. Kesler, M. Lachab, B. Zhang, A. Heidari, H. Nazir, I. Ahmad, J. Dion, Q. Fareed, V. Adivarahan, M. Islam, A. Khan, Appl. Phys. Express 4 (2011) 032102.
[3] D.G. Zhao, S. Zhang, D.S. Jiang, J.J. Zhu, Z.S. Liu, H. Wang, S.M. Zhang, B.S. Zhang, H. Yang, J. Appl. Phys. 110 (2011) 053701.
[4] M.L. Nakarmi, B. Cai, J.Y. Lin, H.X. Jiang, Phys. Stat. Sol. A 209 (2012) 126.
[5] J. Bai, T. Wang, P.J. Parbrook, K.B. Lee, A.G. Cullis, J. Crystal Growth 282 (2005) 290.
[6] J. Bai, M. Dudley, W.H. Sun, H.M. Wang, M.A. Khan, Appl. Phys. Lett. 88 (2006) 051903.
[7] A.V. Sampath, G.A. Garrett, C.J. Collins, W.L. Sarney, E.D. Readinger, P.G. Newman, H. Shen, M. Wraback, J. Electron. Materials 35 (2006) 641.
[8] V.N. Jmerik, A.M. Mizerov, A.A. Sitnikova, P.S. Kop'ev, S.V. Ivanov, E.V. Lutsenko, N.P. Tarasuk, N.V. Rzheutskii, G.P. Yablonskii, Appl. Phys. Lett. 96 (2010) 141112.
[9] Y. Liao, C. Thomidis, C.-K. Kao, T.D. Moustakas, Appl. Phys. Lett. 98 (2011) 081110.
[10] A.V. Tikhonov, T.V. Malin, K.S. Zhuravlev, L. Dobos, B. Pecz, J. Crystal Growth 338 (2012) 30.
[11] D. Litvinov, D. Gerthsen, R. Vohringer, D.Z. Hub, D.M. Schaadt, J. Crystal Growth 338 (2012) 283.
[12] V.N. Jmerik, A.M. Mizerov, D.V. Nechaev, P.A. Aseev, A.A. Sitnikova, S.I. Troshkov, P.S. Kop'ev, S.V. Ivanov, J. Crystal Growth 354 (2012) 188.
[13] M.A. Moram, M.E. Vickers, Rep. Prog. Phys. 72 (2009) 036502.
[14] L.W. Sang, Z.X. Qin, H. Fang, T. Dai, Z.J. Yang, B. Shen, G.Y. Zhang, X.P. Zhang, J. Xu, D.P. Yu, Appl. Phys. Lett. 93 (2008) 122104.
[15] Z. Ren, Q. Sun, S.-Y. Kwon, J. Han, K. Davitt, Y.K. Song, A.V. Nurmikko, H.-K. Cho, W. Liu, J.A. Smart, L.J. Schowalter, Appl. Phys. Lett. 91 (2007) 051116.